

Monitoring Self-Assembly and Ligand Exchange of PbS Nanocrystal Superlattices at the Liquid/Air Interface in Real Time

Santanu Maiti,^{†,‡} Alexander André,^{‡,§} Rupak Banerjee,^{§,¶} Jan Hagenlocher,[†] Oleg Kononov,^{||} Frank Schreiber,^{†,⊥} and Marcus Scheele^{*,‡,⊥}

[†]Institute of Applied Physics, University of Tübingen, Auf der Morgenstelle 10, 72076 Tübingen, Germany

[‡]Institute of Physical and Theoretical Chemistry, University of Tübingen, Auf der Morgenstelle 18, 72076 Tübingen, Germany

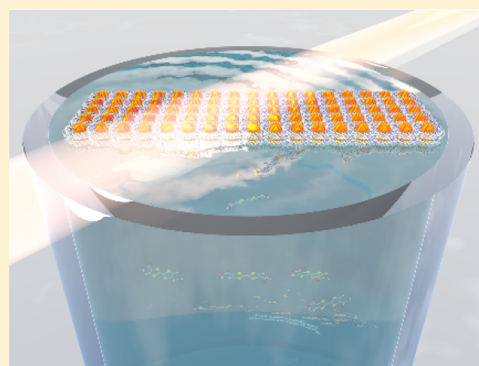
[§]Department of Physics, Indian Institute of Technology Gandhinagar, Palaj, Gandhinagar 382355, India

^{||}Beamline ID10, European Synchrotron Radiation Facility (ESRF), Grenoble F-38043, France

[⊥]Center for Light–Matter Interaction, Sensors & Analytics LISA+, University of Tübingen, Auf der Morgenstelle 15, 72076 Tübingen, Germany

Supporting Information

ABSTRACT: We investigate in situ the structural changes during self-assembly of PbS nanocrystals from colloidal solution into superlattices, solvent evaporation, and ligand exchange at the acetonitrile/air interface by grazing incidence small-angle X-ray scattering (GISAXS). We simulate and fit the diffraction peaks under the distorted wave Born approximation (DWBA) to determine the lattice parameters. We observe a continuous isotropic contraction of the superlattice in two different assembly steps, preserving the body-centered cubic lattice with an overall decrease in the lattice constants of 11%. We argue that the first contraction period is due to a combination of solvent evaporation/annealing and capillary forces acting on the superlattice, whereas the second period is dominated by the effect of replacing oleic acid on the nanocrystal surface with the short and rigid cross-linker tetrathiafulvalene dicarboxylate. This work provides guidelines for optimized ligand exchange conditions and highlights the structural particularities arising from assembling NCs on liquid surfaces.



Self-assembly of semiconductor nanocrystals (NCs) into ordered and conductive superlattices is anticipated to lead to coupled supercrystals and even mini-band formation, with entirely new physical properties.^{1–8} Because as-synthesized NCs are usually poorly conductive due to their insulating ligand shell, exchange procedures with conductive ligands have been extensively investigated.^{9,10} Effective strategies include ligand exchange before, after, or during self-assembly of NCs into ordered superlattices, which are typically characterized by X-ray scattering techniques.^{11–15} Performing such experiments in situ allows elucidation of the complex structural evolution of the superlattice during assembly and ligand exchange, which is usually carried out on solid substrates or in suspended droplets.^{16–20} In situ X-ray studies can also be conducted at the liquid surface, which requires the necessary infrastructure for tilting the X-ray beam rather than the substrate.^{21–28} Due to the strong capillary waves and forces operative at liquid surfaces, it has been suggested that self-assembly of NCs under these conditions may be mechanistically distinct from the superlattice formation during drying of thin liquid films on solids.^{29,30} In view of the growing importance of the liquid/air interface method for the fabrication of conductive NC superlattices, elucidating the mechanistic particularities of this

procedure is important for the rational design of NC superlattices with tailored electronic properties.

Here, we study self-assembly of oleic acid (OA)-stabilized, 6.8 ± 0.2 nm PbS NCs from hexane:octane (1:1) solution at the acetonitrile/air interface followed by ligand exchange with the organic semiconductor (OSC) molecule tetrabutylammonium tetrathiafulvalenedicarboxylate ($[\text{TBA}]_2\text{TTFDA}$) in situ and determine the structural evolution.³¹ We arrive at three core conclusions: (1) The superlattice contracts isotropically during both processes by preserving the initial structure with an 11% reduction in the lattice constant. (2) Roughly half of this shrinkage occurs during self-assembly due to interdigitation and/or vapor annealing, while the other half is due to exchange with the smaller OSC molecule. (3) The final interparticle spacing is precisely one molecular length of the bidentate TTFDA molecule, suggesting that it is acting as a rigid cross-linker between adjacent NCs. This is corroborated by the fact that the interparticle distance does not change upon transferring the superlattice from the liquid to a solid substrate, in

Received: December 11, 2017

Accepted: January 24, 2018

Published: January 24, 2018

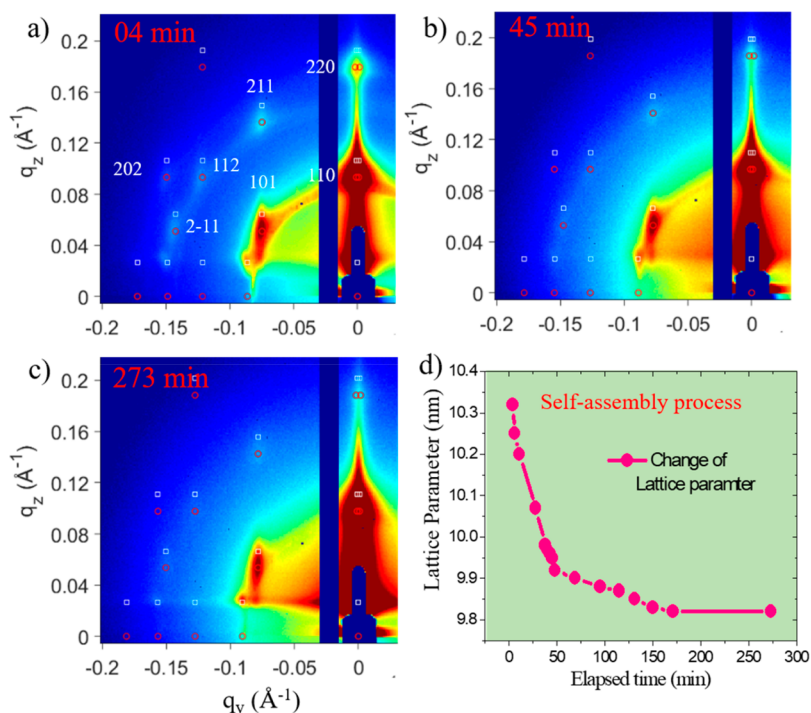


Figure 1. (a–c) In situ GISAXS patterns monitoring the self-assembly without ligand exchange (the elapsed time is marked in red). Red circles (transmitted) and white boxes (reflected) denote simulated diffraction peaks of a bcc superlattice with $[110]$ orientation and $Im\bar{3}m$ SG symmetry. All GISAXS patterns at different times can be indexed with the same reflection planes as marked in (a). (d) Temporal evolution of the bcc lattice constant.

contrast to previous reports operating with monovalent surface molecules.²⁵

Self-Assembly into Superlattices without Ligand Exchange. While details are provided as [Supporting Information](#), in brief, the self-assembly into superlattices was invoked by dispersing $\sim 200 \mu\text{L}$ of a 1:1 hexane:octane solution with a concentration of $3.3 \mu\text{M}$ of PbS NCs on top of acetonitrile with a surface area of 12 cm^2 . The NCs were capped with an OA-ligand shell of initially roughly 3 molecules/ nm^2 . Typical in situ GISAXS patterns for these unexchanged superlattices are presented in [Figure 1a–c](#), simulated with the distorted wave Born approximation (DWBA) and fitted to extract the lattice parameters ([Table S1](#)). We find that all of the GISAXS patterns fit well to a body-centered cubic (bcc) superlattice with ($Im\bar{3}m$) space group (SG) symmetry, an initial lattice constant of $a = (10.3 \pm 0.02) \text{ nm}$, and a $[110]$ orientation normal to the substrate. As evident in [Figure 1d](#), the lattice contracts from 10.3 to 9.9 nm during the first 45 min, followed by a very small ($\sim 0.1 \text{ nm}$) contraction during the remaining measurement time to result in a 5% overall contraction of the superlattice.

We use here the DWBA to simulate the diffraction patterns because of the particular challenges inherent to interpreting GISAXS patterns as in grazing incidence the scattering intensity is affected by multiple scattering–reflection events.^{32,33} In contrast to the simpler Born approximation (BA), the DWBA method is based on first-order perturbation theory and treats structures like NCs, islands, and roughness as small perturbations to a potential landscape of the perfectly flat surface.^{34,35} In effect, the incident, reflected, and refracted waves interfere and give rise to an effective form factor, affecting each component of the momentum transfer in q -space and thus the resulting scattering pattern. To obtain this effective form factor, one needs to consider the electron density

(ED) as well as the critical angle of the NC superstructures with respect to the substrates (liquid or solids), which ultimately determine the scattered pathways of X-rays with the varied refractive index of the system. We estimate these parameters from the X-ray reflectivity (XRR) profiles, obtained at different time intervals during the assembly processes ([Figures S3 and S5](#)), and incorporate them into the respective simulations.

Self-Assembly into Superlattices Followed by Ligand Exchange. In situ GISAXS measurements of NCs self-assembled on the liquid surface followed by ligand exchange with TTFDA are presented in [Figure 2](#). After dispersing the NCs (-40 min) onto the acetonitrile surface, the NCs self-assemble during the first waiting period of 46 min with the same lattice constant and kinetics as those observed in [Figure 1d](#). After injecting TTFDA, the representative GISAXS patterns obtained at +08, +153, and +188 min are shown in [Figure 2b–d](#) (and other intermediate time frames in [Figure S4](#)). All patterns at seven different assembling times after ligand injection show a high resemblance to the previous in [Figures 1 and 2a](#), indicating that neither the self-assembly nor the ligand exchange processes noticeably alters the symmetry of the superlattice. A lattice parameter of 9.6, 9.25, and 9.2 nm is observed at +08, +153 and +188 min of elapsed time after the ligand injection ($t = 0$) and upon fitting of the corresponding patterns with bcc (SG: $Im\bar{3}m$) superlattice symmetry. The plot of the evaluated lattice parameters ([Table S2](#)) as a function of elapsed measurement time before and after ligand injection is presented in [Figure 2e](#), illustrating that the superlattice contracts significantly further than what we observed without ligand exchange.

To visualize the contraction of the unit cell as a function of assembling/reaction time, we present the line profiles of the two most prominent (110) and (101) reflections along the out-

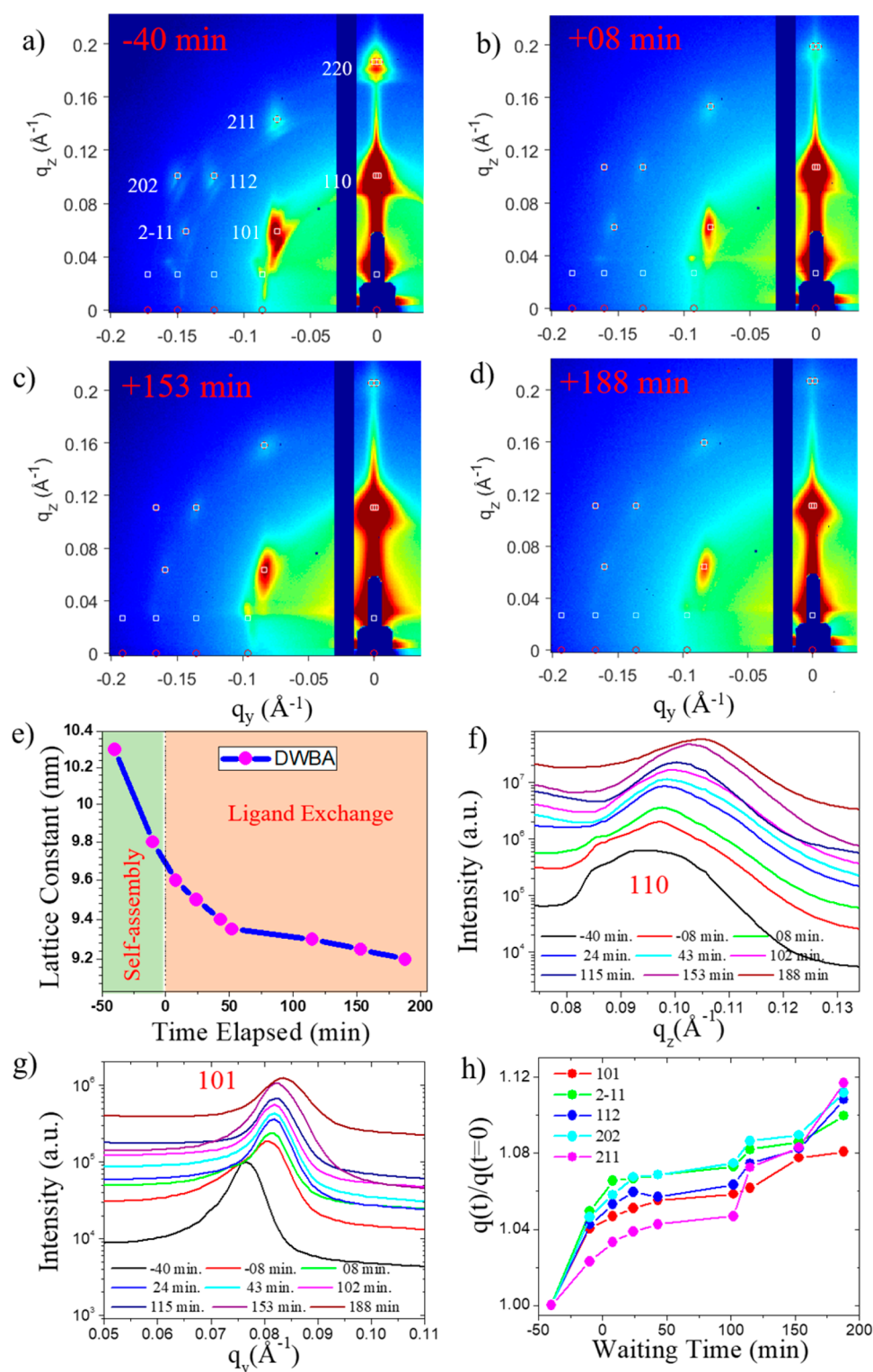


Figure 2. GISAXS patterns during the assembly process with elapsed times marked at the left corner of each image (a) before and (b-d) after ligand injection. White boxes \square (reflected) and red circles (transmitted) are the simulated diffraction patterns for a bcc superlattice with [110] orientation and $Im\bar{3}m$ SG symmetry. All patterns can be indexed with the same reflection planes as marked in (a). (e) Temporal evolution of the bcc lattice constant. (f) Out-of-plane line profiles along q_z through the (110) truncation rods (at $q_y = 0$) for GISAXS patterns obtained at nine different assembling/reaction times (-40, -08, +08, +24, +43, +102, +115, +153, +188 min). (g) In-plane line profiles along q_y through the (101) truncation rods (at $q_z = 0.06 \text{\AA}^{-1}$) for GISAXS patterns obtained at nine different corresponding assembling times. Peak intensities have been scaled up for clarity. (h) Temporal evolution of the normalized ($q(t)/q(t=0)$) q_y -values for all five reflections visible in the scattering pattern in (a).

of-plane (q_z) and in-plane (q_y) directions of the bcc superlattice in Figure 2f,g, respectively. Similar results are obtained for all other out-of-plane and in-plane reflections marked in Figure 2a

(see Figure S6 in the SI for details). The relative shift of each peak position at higher q values with elapsed time clearly depicts the ongoing contraction. We attribute the additional 6%

contraction in the lattice constant from 9.8 to 9.2 nm to the effect of exchanging the relatively large OA ligand with the shorter TTFDA molecules. We note that vibrational spectroscopy of the superlattice retrieved after the experiment suggests a near-complete ligand exchange based on the disappearance of the sp^3 C–H vibrations. To illustrate the isotropic nature of the unit cell contractions in the thick layer, we plot the temporal evolution of the total momentum transfer $q(t)$ with respect to the initial $q(t = 0)$ for five different diffraction peaks in Figure 2h. We find practically identical behavior for all five peaks, which again confirms the continuous contraction of the unit cell during self-assembly and ligand exchange.

We now compare the results of our work with other *in situ* studies of the self-assembly of NCs on liquid surfaces. Geuchis et al. observed a structural transformation from quasi-hexagonal close-packed into square superlattices during self-assembly on ethylene glycol.²¹ This was attributed to necking and partial fusion of the NCs during solvent evaporation. However, while ethylene glycol is well-known to induce ligand stripping from NC surfaces, acetonitrile (applied in the present work) has been shown to leave lead chalcogenide surfaces largely intact.³⁶ van der Stam et al. reported on oleylamine (Olm)-capped ZnS NCs assembled into superlattices on ethylene glycol in the presence of OA.²⁵ The authors found an in-plane contraction by 1.8 nm without adding OA and 1.5 nm in the presence of OA. This was attributed to the interdigitization/buckling of surface ligands during solvent evaporation. We note again that acetonitrile reportedly removes much fewer ligands from the PbS surface, which may explain why the contraction during drying in our work is significantly smaller.³⁶ In addition, a possible buckling in the structure would likely manifest in a change of the in-plane scattering truncation rod into an “arc” shape, which we do not observe here.³⁷

In contrast, we briefly discuss a few alternative explanations, which we deem more likely to be held responsible for the observed contraction during self-assembly and solvent evaporation on the liquid surface without ligand exchange (Figure 1 and the period from –40 to 0 min in Figure 2). We argue that this contraction is due to continuous interdigitization of OA ligands during evaporation of the solvent and/or simultaneous self-vapor-annealing as the cell was mostly closed throughout the experiment.^{38,39} The volatile carrier solvent (1:1 hexane/octane) of the NCs evaporates over ~46 min and fills the closed chamber with vapor. The drop of intensity in the scattering pattern in Figure 1b is supporting evidence for this scenario. As the NCs are partially immersed into the liquid, one also has to consider immersion-induced effects.^{40–42} Thermal fluctuation forces (capillary waves)^{29,41} are always present at the liquid surface along with capillary forces, which are foremost the result of NCs immersing into the acetonitrile phase, inducing the assembly to conserve the structural symmetry.^{42,43} In this regard, it is worth noting that the ligand-stabilized NCs may have also other important parameters because of their complex surfaces, different facets with varying ligand densities and binding motifs.⁴⁴ Such surface parameters or anisotropy may also lead to the formation of multipoles at the liquid/air/NC interface and additional interparticle attractive forces.^{30,45}

In continuation of comparing the present work with the results by van der Stam et al., we now discuss the origin of the additional contraction observed after initiating ligand exchange with TTFDA (the period starting at “0 min” in Figure 2). TTFDA is a fully conjugated molecule with an sp^2 -hybridized

carbon backbone in contrast to OA or Olm, which are mostly sp^3 -hybridized and flexible. In addition, only TTFDA with anchoring groups on both sides of the molecule is capable of cross-linking adjacent NCs. Therefore, TTFDA-capped NCs are likely to exhibit some structural rigidity in the ligand shell and cannot easily undergo further structural changes once the interparticle distance is on the order of one TTFDA molecule (1.1 nm). In view of the NC diameter of 6.8 ± 0.2 nm and an extracted interparticle distance (given by the half-diagonal of the bcc cell) of 7.9 nm for the fully exchanged NC superstructure (Figure 2e), we find that this limit may indeed be reached here (1.1 nm). We sought to test this hypothesis by recovering the ligand-exchanged superlattice from the liquid surface and drying it on a solid support. A comparison of the in-plane line profiles through the (011) lattice planes of the corresponding GISAXS patterns in Figure 3a reveal no change

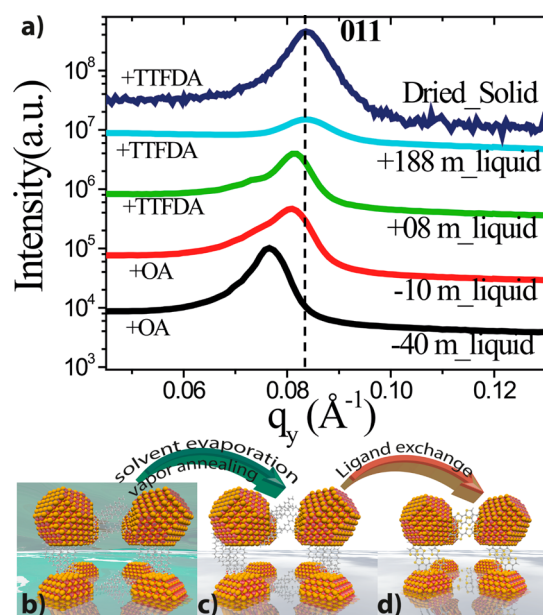


Figure 3. (a) Comparison of the temporal evolution of the superlattice during contraction period 1 (“+8 min”), period 2 (“+188 min”), and after retrieval and drying of the NC superlattice (“dried”) along the in-plane direction (resembled by q_y of the (011) reflection). (c–e) Idealized schematics of the proposed sequential contraction of the PbS superlattice upon drying on an acetonitrile surface and ligand exchange with TTFDA. (b) In the beginning of the experiment, OA-capped PbS NCs begin to form a superlattice with bcc structure, while the solvent (indicated by the green color) has not completely dried. (c) In contraction period 1, complete drying of the NCs on the acetonitrile liquid leads to a lateral contraction of the superlattice. At this point, the NCs are still capped with OA, acting as flexible spacers. (d) In contraction period 2, OA is replaced by TTFDA, triggering further contraction of the superlattice.

before and after this transfer. This is in contrast to the results of a similar experiment performed by van der Stam et al. with the monodentate molecules OA and Olm.²⁵ We take this as evidence that the seemingly reversible superlattice contraction at the liquid/air interface can be “locked-in” by cross-linking adjacent NCs with a rigid, bidentate molecule like TTFDA.

Our complete view of the sequential isotropic contraction of a 3D superlattice on the liquid surface in this work is schematically depicted in Figure 3b–d. Particularly noteworthy is that the bcc symmetry of the NCs superlattice is conserved throughout the self-assembly processes, undergoing different

physical/chemical effects with elapsed time. The first 5% contraction before ligand exchange is mainly due to solvent evaporation/annealing and the effect of capillary forces (from (b) to (c)). Ligand exchange with TTFDA (from (c) to (d)) invokes an additional 6% contraction due to near-complete exchange and the shorter molecular length of TTFDA compared to that of OA.

In summary, we have investigated the self-assembly of PbS NCs into multilayered superlattices at the acetonitrile/air interface in real time by grazing incidence small-angle X-ray scattering. We used the bidentate cross-linker tetrathiafulvalene dicarboxylate to exchange the native OA surface ligands and monitored the structural changes to the superlattices in situ. We arrive at three core findings: (1) The superlattice contracts isotropically during solvent evaporation and ligand exchange by preserving the initial structure with an 11% decreased lattice constant. (2) Roughly half of this decrease occurs during self-assembly due to interdigitation and/or vapor annealing, while the other half is due to exchange with the smaller cross-linker. (3) The final interparticle spacing is precisely one molecular length of the bidentate TTFDA molecule, suggesting that it rigidly connects adjacent NCs. Our work is intended to help improve the structural coherence in NC superlattices and provide guidelines for optimized ligand exchange conditions and highlights the structural differences arising from assembling NCs on liquid surfaces.

■ ASSOCIATED CONTENT

Supporting Information

The Supporting Information is available free of charge on the ACS Publications website at DOI: 10.1021/acs.jpclett.7b03278.

Figures S1–S12, showing the apparatus, GISAXS patterns, temporal evolution of the XRR profile, complete analysis of the reflections, the chemical structure of deprotonated TTFDA, XRR data, determination of the evaporation rate and surface height variation, vis/IR absorption plots and TEM images, and AFM images; Tables S1 and S2, giving parameters of the self-assembly; experimental procedures; and further material characterization (PDF)

■ AUTHOR INFORMATION

Corresponding Author

*E-mail: marcus.scheele@uni-tuebingen.de.

ORCID

Rupak Banerjee: 0000-0002-1189-1502

Marcus Scheele: 0000-0002-2704-3591

Author Contributions

#S.M. and A.A. contributed equally to the publication.

Notes

The authors declare no competing financial interest.

■ ACKNOWLEDGMENTS

This work was supported by the DFG under Grants SCHE1905/3, SCHE1905/4, and SCHR700/25. We thank the European Synchrotron Radiation Facility (ESRF), Grenoble, France, for enabling X-ray diffraction experiments at beamline ID10. The synthesis of TTFDA was performed as a user projects at the Molecular Foundry, which was supported by the Office of Science, Office of Basic Energy Sciences, of the U.S. Department of Energy under Contract No. DE-AC02-

05CH11231. R.B. would like to thank the Department of Science and Technology, India (SR/NM/Z-07/2015) for the financial support and Jawaharlal Nehru Centre for Advanced Scientific Research (JNCASR) for managing the project. We also thank Mrs. Elke Nadler, Institute of Physical and Theoretical Chemistry, University of Tübingen, for performing SEM/STEM measurements using a Hitachi SU 8030 SEM, which was funded by the DFG under Contract INST 37/829-1 FUGG, partially.

■ REFERENCES

- (1) Artemyev, M. V.; Bibik, A. I.; Gurinovich, L. I.; Gaponenko, S. V.; Woggon, U. Evolution from Individual to Collective Electron States in a Dense Quantum Dot Ensemble. *Phys. Rev. B: Condens. Matter Mater. Phys.* **1999**, *60*, 1504–1506.
- (2) Boles, M. A.; Engel, M.; Talapin, D. V. Self-Assembly of Colloidal Nanocrystals: From Intricate Structures to Functional Materials. *Chem. Rev.* **2016**, *116*, 11220–11289.
- (3) Carnello, M.; Johnston-Peck, A. C.; Diroll, B. T.; Wong, E.; Datta, B.; Damodhar, D.; Doan-Nguyen, V. V. T.; Herzing, A. A.; Kagan, C. R.; Murray, C. B. Substitutional Doping in Nanocrystal Superlattices. *Nature* **2015**, *524*, 450–453.
- (4) Döllefeld, H.; Weller, H.; Eychemüller, A. Semiconductor Nanocrystal Assemblies: Experimental Pitfalls and a Simple Model of Particle-Particle Interaction. *J. Phys. Chem. B* **2002**, *106*, 5604–5608.
- (5) Hanrath, T. Colloidal Nanocrystal Quantum Dot Assemblies as Artificial Solids. *J. Vac. Sci. Technol., A* **2012**, *30*, 030802.
- (6) Kagan, C. R.; Murray, C. B.; Bawendi, M. G. Long-Range Resonance Transfer of Electronic Excitations in Close-Packed CdSe Quantum-Dot Solids. *Phys. Rev. B: Condens. Matter Mater. Phys.* **1996**, *54*, 8633–8643.
- (7) Lazarenkova, O. L.; Balandin, A. A. Miniband Formation in a Quantum Dot Crystal. *J. Appl. Phys.* **2001**, *89*, 5509–5515.
- (8) Vanmaekelbergh, D. Self-Assembly of Colloidal Nanocrystals as Route to Novel Classes of Nanostructured Materials. *Nano Today* **2011**, *6*, 419–437.
- (9) Boles, M. A.; Ling, D.; Hyeon, T.; Talapin, D. V. The Surface Science of Nanocrystals. *Nat. Mater.* **2016**, *15*, 141–153.
- (10) Zaluzhnyy, I. A.; Kurta, R. P.; André, A.; Gorobtsov, O. Y.; Rose, M.; Skopintsev, P.; Besedin, I.; Zozulya, A. V.; Sprung, M.; Schreiber, F. Quantifying Angular Correlations between the Atomic Lattice and the Superlattice of Nanocrystals Assembled with Directional Linking. *Nano Lett.* **2017**, *17*, 3511–3517.
- (11) André, A.; Theurer, C.; Lauth, J.; Maiti, S.; Hodas, M.; Samadi Khoshkhoo, M.; Kinge, S.; Meixner, A. J.; Schreiber, F.; Siebbeles, L. D. A. Structure, Transport and Photoconductance of Pbs Quantum Dot Monolayers Functionalized with a Copper Phthalocyanine Derivative. *Chem. Commun.* **2017**, *53*, 1700–1703.
- (12) Dong, A.; Jiao, Y.; Milliron, D. J. Electronically Coupled Nanocrystal Superlattice Films by in Situ Ligand Exchange at the Liquid-Air Interface. *ACS Nano* **2013**, *7*, 10978–10984.
- (13) Kovalenko, M. V.; Scheele, M.; Talapin, D. V. Colloidal Nanocrystals with Molecular Metal Chalcogenide Surface Ligands. *Science* **2009**, *324*, 1417–1420.
- (14) Santra, P. K.; Palmstrom, A. F.; Tassone, C. J.; Bent, S. F. Molecular Ligands Control Superlattice Structure and Crystallite Orientation in Colloidal Quantum Dot Solids. *Chem. Mater.* **2016**, *28*, 7072–7081.
- (15) Weidman, M. C.; Yager, K. G.; Tisdale, W. A. Interparticle Spacing and Structural Ordering in Superlattice Pbs Nanocrystal Solids Undergoing Ligand Exchange. *Chem. Mater.* **2015**, *27*, 474–482.
- (16) Agthe, M.; Plivelic, T. S.; Labrador, A.; Bergstrom, L.; Salazar-Alvarez, G. Following in Real Time the Two-Step Assembly of Nanoparticles into Mesocrystals in Levitating Drops. *Nano Lett.* **2016**, *16*, 6838–6843.
- (17) Bahadur, J.; Sen, D.; Mazumder, S.; Santoro, G.; Yu, S.; Roth, S. V.; Melnichenko, Y. B. Colloidal Nanoparticle Interaction Transition

During Solvent Evaporation Investigated by in-Situ Small-Angle X-Ray Scattering. *Langmuir* **2015**, *31*, 4612–4618.

(18) Ocier, C. R.; Smilgies, D. M.; Robinson, R. D.; Hanrath, T. Reconfigurable Nanorod Films: An in Situ Study of the Relationship between the Tunable Nanorod Orientation and the Optical Properties of Their Self-Assembled Thin Films. *Chem. Mater.* **2015**, *27*, 2659–2665.

(19) Siffalovic, P.; Majkova, E.; Chitu, L.; Jergel, M.; Luby, S.; Satka, A.; Roth, S. V. Self-Assembly of Iron Oxide Nanoparticles Studied by Time-Resolved Grazing-Incidence Small-Angle X-Ray Scattering. *Phys. Rev. B: Condens. Matter Mater. Phys.* **2007**, *76*, 195432.

(20) Weidman, M. C.; Smilgies, D. M.; Tisdale, W. A. Kinetics of the Self-Assembly of Nanocrystal Superlattices Measured by Real-Time in Situ X-Ray Scattering. *Nat. Mater.* **2016**, *15*, 775–781.

(21) Geuchies, J. J.; van Overbeek, C.; Evers, W. H.; Goris, B.; de Backer, A.; Gantapara, A. P.; Rabouw, F. T.; Hilhorst, J.; Peters, J. L.; Konovalov, O. In Situ Study of the Formation Mechanism of Two-Dimensional Superlattices from PbSe Nanocrystals. *Nat. Mater.* **2016**, *15*, 1248–1254.

(22) Maiti, S.; Sanyal, M. K.; Jana, M. K.; Runge, B.; Murphy, B. M.; Biswas, K.; Rao, C. N. R. Evidence of Contact Epitaxy in the Self-Assembly of Hgse Nanocrystals Formed at a Liquid-Liquid Interface. *J. Phys.: Condens. Matter* **2017**, *29*, 095101.

(23) Maiti, S.; Sanyal, M. K.; Varghese, N.; Satpati, B.; Dasgupta, D.; Daillant, J.; Carriere, D.; Konovalov, O.; Rao, C. N. R. Formation of Single-Crystalline CuS at the Organic-Aqueous Interface. *J. Phys.: Condens. Matter* **2013**, *25*, 395401.

(24) Narayanan, S.; Wang, J.; Lin, X. M. Dynamical Self-Assembly of Nanocrystal Superlattices During Colloidal Droplet Evaporation by in Situ Small Angle X-Ray Scattering. *Phys. Rev. Lett.* **2004**, *93*, 135503.

(25) Van der Stam, W.; Rabouw, F. T.; Vonk, S. J. W.; Geuchies, J. J.; Ligthart, H.; Petukhov, A. V.; de Mello Donega, C. Oleic Acid-Induced Atomic Alignment of Zns Polyhedral Nanocrystals. *Nano Lett.* **2016**, *16*, 2608–2614.

(26) Walravens, W.; De Roo, J.; Drijvers, E.; ten Brinck, S.; Solano, E.; Dendooven, J.; Detavernier, C.; Infante, I.; Hens, Z. Chemically Triggered Formation of Two-Dimensional Epitaxial Quantum Dot Superlattices. *ACS Nano* **2016**, *10*, 6861–6870.

(27) Zhang, D. T.; Hu, J. Y.; Kennedy, K. M.; Herman, I. P. Forming Nanoparticle Monolayers at Liquid Air Interfaces by Using Miscible Liquids. *Langmuir* **2016**, *32*, 8467–8472.

(28) Zhang, D. T.; Lu, C.; Hu, J.; Lee, S. W.; Ye, F.; Herman, I. P. Small Angle X-Ray Scattering of Iron Oxide Nanoparticle Monolayers Formed on a Liquid Surface. *J. Phys. Chem. C* **2015**, *119*, 10727–10733.

(29) Sanyal, M. K.; Sinha, S. K.; Huang, K. G.; Ocko, B. M. X-Ray-Scattering Study of Capillary-Wave Fluctuations at a Liquid Surface. *Phys. Rev. Lett.* **1991**, *66*, 628–631.

(30) Soligno, G.; Dijkstra, M.; van Roij, R. Self-Assembly of Cubes into 2D Hexagonal and Honeycomb Lattices by Hexapolar Capillary Interactions. *Phys. Rev. Lett.* **2016**, *116*, 258001.

(31) André, A.; Zhrebetskyy, D.; Hanifi, D.; He, B.; Samadi Khoshkhoo, M.; Jankowski, M.; Chassé, T.; Wang, L.-W.; Schreiber, F.; Salleo, A. Toward Conductive Mesocrystalline Assemblies: Pbs Nanocrystals Cross-Linked with Tetrathiafulvalene Dicarboxylate. *Chem. Mater.* **2015**, *27*, 8105–8115.

(32) Jiang, Z. GIXSGUI: A Matlab Toolbox for Grazing-Incidence X-Ray Scattering Data Visualization and Reduction, and Indexing of Buried Three-Dimensional Periodic Nanostructured Films. *J. Appl. Crystallogr.* **2015**, *48*, 917–926.

(33) Tate, M. P.; Urade, V. N.; Kowalski, J. D.; Wei, T.-C.; Hamilton, B. D.; Eggiman, B. W.; Hillhouse, H. W. Simulation and Interpretation of 2d Diffraction Patterns from Self-Assembled Nanostructured Films at Arbitrary Angles of Incidence: From Grazing Incidence (above the Critical Angle) to Transmission Perpendicular to the Substrate. *J. Phys. Chem. B* **2006**, *110*, 9882–9892.

(34) Renaud, G.; Lazzari, R.; Leroy, F. Probing Surface and Interface Morphology with Grazing Incidence Small Angle X-Ray Scattering. *Surf. Sci. Rep.* **2009**, *64*, 255–380.

(35) Sinha, S. K.; Sirota, E. B.; Garoff, S.; Stanley, H. B. X-Ray and Neutron-Scattering from Rough Surfaces. *Phys. Rev. B: Condens. Matter Mater. Phys.* **1988**, *38*, 2297–2311.

(36) Hassinen, A.; Moreels, I.; de Nolf, K.; Smet, P. F.; Martins, J. C.; Hens, Z. Short-Chain Alcohols Strip X-Type Ligands and Quench the Luminescence of PbSe and CdSe Quantum Dots, Acetonitrile Does Not. *J. Am. Chem. Soc.* **2012**, *134*, 20705–20712.

(37) Bera, M. K.; Sanyal, M. K.; Pal, S.; Daillant, J.; Datta, A.; Kulkarni, G. U.; Luzet, D.; Konovalov, O. Reversible Buckling in Monolayer of Gold Nanoparticles on Water Surface. *EPL* **2007**, *78*, 56003–6.

(38) Bian, K.; Choi, J. J.; Kaushik, A.; Clancy, P.; Smilgies, D.-M.; Hanrath, T. Shape-Anisotropy Driven Symmetry Transformations in Nanocrystal Superlattice Polymorphs. *ACS Nano* **2011**, *5*, 2815–2823.

(39) Rabani, E.; Reichman, D. R.; Geissler, P. L.; Brus, L. E. Drying-Mediated Self-Assembly of Nanoparticles. *Nature* **2003**, *426*, 271–274.

(40) Bresme, F.; Oettel, M. Nanoparticles at Fluid Interfaces. *J. Phys.: Condens. Matter* **2007**, *19*, 413101.

(41) Fleck, N. A.; McMeeking, R. M.; Kraus, T. Convective Assembly of a Particle Monolayer. *Langmuir* **2015**, *31*, 13655–13663.

(42) He, A.; Nguyen, K.; Mandre, S. Capillary Interactions between Nearby Interfacial Objects. *EPL* **2013**, *102*, 38001.

(43) Daillant, J.; Belorgey, O. Surface Scattering of X-Rays in Thin-Films. Part II. Experiments on Thin Soap Films. *J. Chem. Phys.* **1992**, *97*, 5837–5843.

(44) Zhrebetskyy, D.; Scheele, M.; Zhang, Y.; Bronstein, N.; Thompson, C.; Britt, D.; Salmeron, M.; Alivisatos, A. P.; Wang, L.-W. Hydroxylation of the Surface of PbS Nanocrystals Passivated with Oleic Acid. *Science* **2014**, *344*, 1380–1384.

(45) Lotito, V.; Zambelli, T. Approaches to Self-Assembly of Colloidal Monolayers: A Guide for Nanotechnologists. *Adv. Colloid Interface Sci.* **2017**, *246*, 217–274.